Geophys. J. Int. (2005) **160,** 736–752 doi: 10.1111/j.1365-246X.2005.02514.x

The crustal structure of central East Greenland—I: From the Caledonian orogen to the Tertiary igneous province

Mechita C. Schmidt-Aursch and Wilfried Jokat

Alfred Wegener Institute for Polar and Marine Research, Columbusstrasse, 27568 *Bremerhaven, Germany*
E-mails: mschmidt@awi-bremerhaven.de (MCSA); wjokat@awi-bremerhaven.de (WJ)

Accepted 2004 October 18. Received 2004 May 5; in original form 2003 July 24

SUMMARY

We present a regional crustal model of the East Greenland Fjord Region between 69°N and 74°N which spans the Caledonian fold belt and the adjoining Devonian and Mesozoic basins. The model is a compilation of existing seismic models that were partly reinterpreted and newly derived results from different modelling approaches. Remodelling of 33 stations on three deep seismic lines in the southern area yielded consistent *P*-wave velocity models for the entire Fjord Region. Seismic velocities, between 5.5 km s^{-1} near the surface and 6.9 km s^{-1} in the lower crust are typical for regions of Palaeozoic age. Moho depths up to 48 km in the seismic models suggest the existence of a crustal root beneath the Caledonian orogen. Shear wave modelling of 51 stations on six refraction seismic profiles resulted in *S*-wave velocities between 3.2 km s^{-1} in the upper crust, 4.0 km s^{-1} at the crust–mantle boundary and 4.2 km s^{-1} in the partial magmatic underplating of the lower crust in the northern area. Calculation of Poisson's ratio portrays a fairly homogeneous crust with only slight variations in Poisson's ratio of 0.26–0.30 for the uppermost crystalline crust and 0.22–0.24 for the middle crust. These values cannot be linked to lithological variations because they are either small-scale or span several tectonic provinces. Finite-difference modelling and amplitude analysis confirm models without magmatic underplating in the lower crust of the southern Hall Bredning, Scoresby Sund area.

Key words: continental crust, crustal structure, East Greenland, seismic refraction.

1 INTRODUCTION

The East Greenland Fjord Region between 69°N and 76°N, together with northeast and southeast Greenland and the coasts of Scandinavia and the British Isles, form the conjugate continental margins of the North Atlantic. The region is mainly shaped by the Caledonian fold belt, formed in Silurian times during the closure of the Iapetus Ocean by continent–continent collision (e.g. Escher & Pulvertaft 1995; Henriksen *et al.* 2000). The western parts of the Greenland Caledonian orogen are covered by a permanent ice sheet and the Caledonian foreland is only exposed in a few tectonic windows. The eastern parts of the Greenland orogen are separated by several faults from sedimentary basins that developed during the ensuing Devonian extensional collapse and long-term rifting (Fig. 1). During the opening of the North Atlantic in Tertiary times, large amounts of flood basalts were generated which obscure the southern termination of the Caledonides at 70°N along the southern coast of Scoresby Sund.

Whereas the European margins were explored at an early stage, the East Greenland side remained geophysically poorly known for a long time. Most early seismic reflection surveys concentrated on the shelf area (see Larsen 1990, for a review) and the Jameson Land Basin (e.g. Larsen & Marcussen 1992). The first seismic refraction surveys were conducted in the region in 1988 (Weigel *et al.* 1995). The long fjords provided good opportunities for land–sea seismic experiments. In the years 1990 and 1994, the Alfred Wegener Institute for Polar and Marine Research (AWI) acquired additional wide-angle seismic lines (Jokat *et al.* 1995, 1996) which yielded detailed velocity models of the continental crust (Fechner & Jokat 1996; Mandler & Jokat 1998; Schlindwein & Jokat 1999). Analyses of gravity and magnetic data complemented the seismic models (Schlindwein & Meyer 1999; Schlindwein & Jokat 2000). Differing interpretations exist in the literature, due to the different databases and working emphasis of the projects in the region. For example, the question of the existence of magmatic underplating of the crust in the Scoresby Sund region has not yet been finally answered.

The objective of this study was to create a regional model for the continental crust of central East Greenland between 69°N and 74°N. For this purpose, a uniform modelling approach for all data sets was attempted. Existing seismic refraction lines were inspected and, as a consequence, the traveltimes of all 33 useable stations on the three profiles in the southern Fjord Region (south of 72°N) were remodelled to reach consistent *P*-wave velocity models. In addition to previous studies, shear wave arrivals were picked on the sections of 51 stations on six profiles in the entire Fjord Region to compile *S*-wave velocity models and to calculate Poisson's ratio. Because

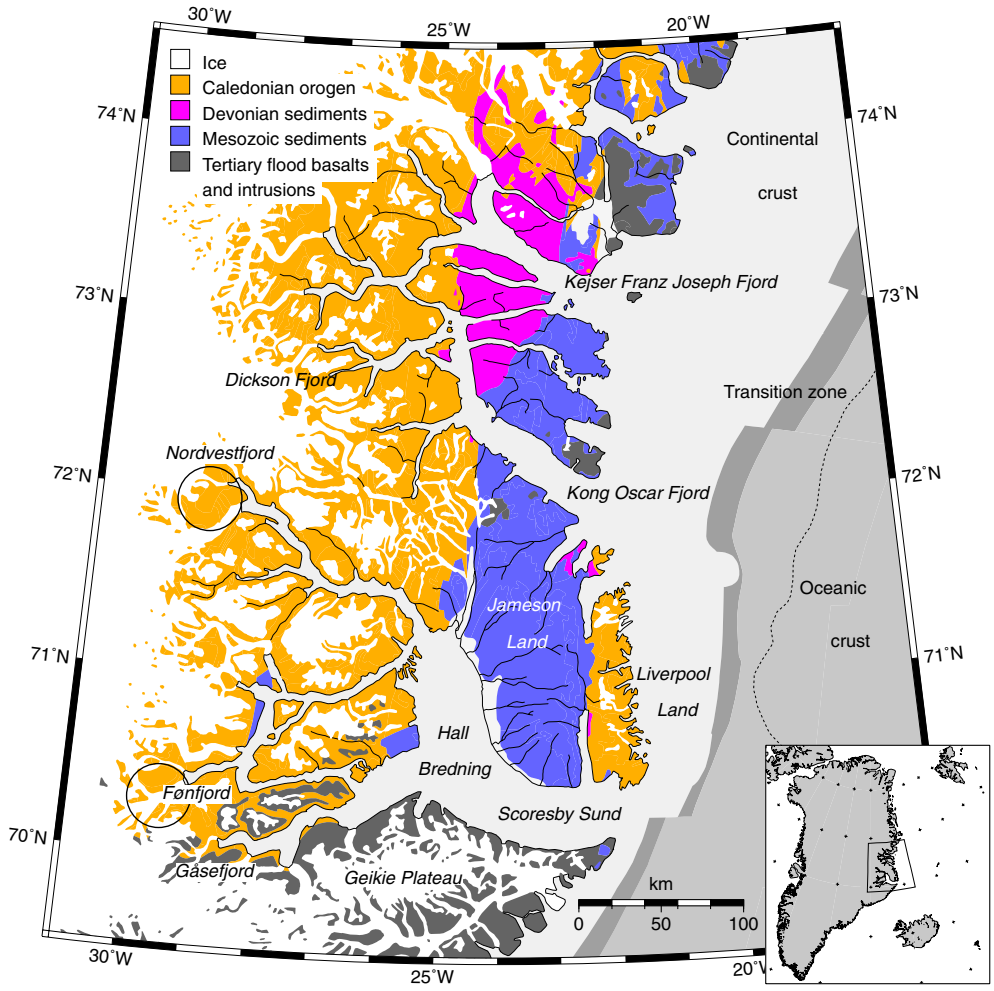

Figure 1. Simplified geological map of the East Greenland Fjord Region after Escher & Pulvertaft (1995) (copyright Geological Survey of Denmark and Greenland) and Henriksen *et al.* (2000). Circles mark areas with Caledonian foreland exposed in tectonic windows. The dashed line indicates the shelf edge.

ray tracing didn't yield a unique solution, finite-difference modelling of selected stations was performed to address the controversy surrounding magmatic underplating in the southern realm. The result of these investigations are presented here. Further work was done by a 3-D gravity modelling to extrapolate the crustal model into adjacent areas. This is presented in an accompanying paper (Schmidt-Aursch & Jokat 2005, this issue).

2 SEISMIC VELOCITY MODELLING

Six wide-angle seismic transects were acquired in the Fjord Region during two expeditions in 1990 and 1994 (Fig. 2 and Table 1). The processing stages of the data and the resulting seismic velocity models (Mandler & Jokat 1998; Schlindwein & Jokat 1999) are too diverse for a regional crustal model. For this reason we revised the three southern profiles in the Scoresby Sund area (Nordvestfjord, Gåsefjord and Fønfjord profiles) and created *P*-wave velocity models, which are not only consistent with themselves but also with the three profiles of the northern Fjord Region (north of 72°N; Kejser Franz Joseph Fjord, Kong Oscar Fjord and Dickson Fjord profiles).

2.1 Modelling method

The curved geometry of the transects along the fjords required the projection of shots and stations onto a straight line (Fig. 2), but the distances between shots and stations, and hence the offsets of traveltime arrivals, were left unchanged. This lead to different ray paths for the real profile and the projected model and, accordingly, to an averaging of laterally inhomogeneous crustal structures. Stations located onshore parallel to the ship's track were projected onto the seafloor and a corresponding static correction to account for rock versus water was applied. The observed seismic traveltimes were corrected for this assuming vertical ray incidence and using a mean seismic velocity typical for the uppermost crust of 5.5 km s^{-1} for *P* waves and 3.2 km s^{-1} for *S* waves, respectively. Traveltime errors arising from the static correction are estimated to be less than ± 0.10 s. Traveltimes of *P*- and *S*-wave arrivals were picked on all seismic recordings and assigned with an estimated error of between ± 0.05 and ± 0.25 s, depending on data quality. For few shear wave arrivals, the estimated error is up to ± 0.5 s.

Two-dimensional (2-D) ray tracing was carried out with the RAYINVR software (Zelt & Smith 1992). Only forward modelling of each layer, from top to bottom, was performed as inversion partly failed due to poor data quality and quantity (e.g. large data gaps, strong undulations due to rough sea floor topography). We concentrated on fitting the slope of traveltime curves rather than on minimizing the residuals. No resolution was calculated, as the model parametrization nodes are not uniformly spaced. Instead, for each layer, the coverage with refracted and reflected rays traced to

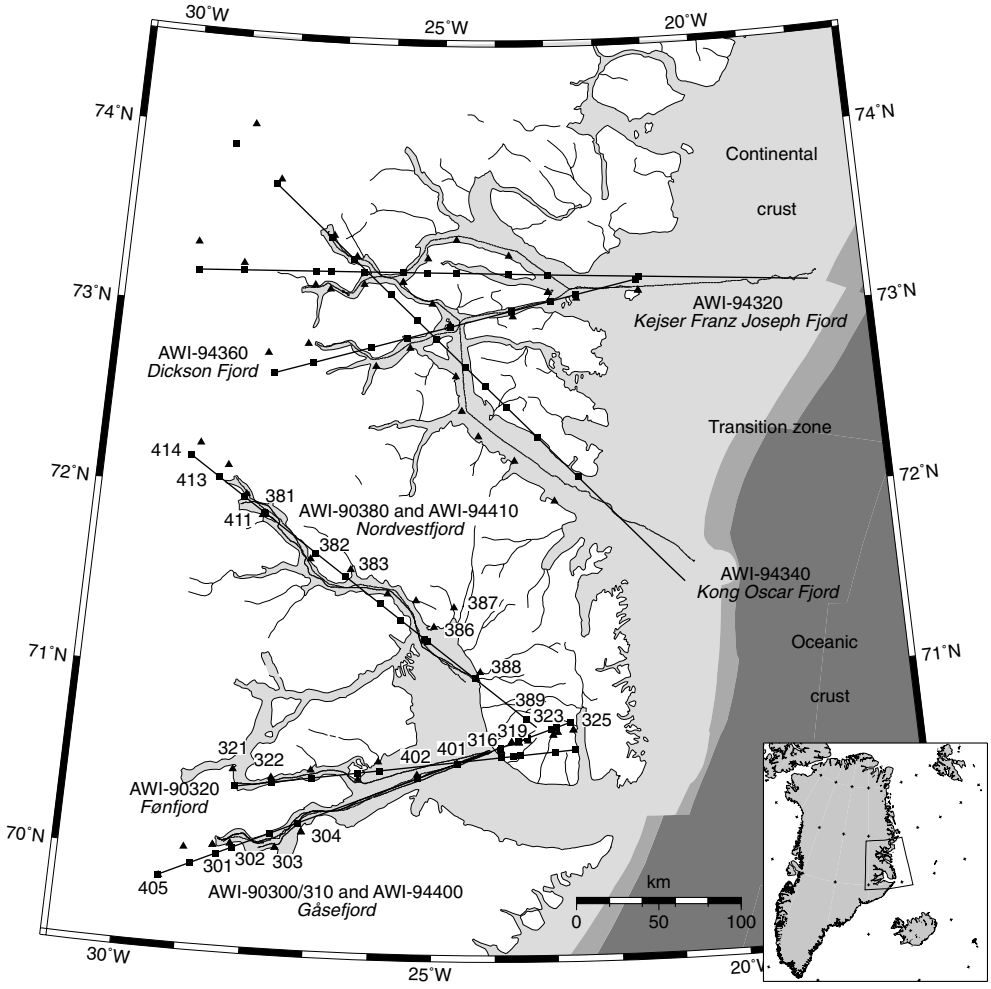

Figure 2. Location of the deep seismic profiles. Thin lines show the ship's tracks and triangles the locations of the recording stations. Bold lines indicate the seismic models, squares mark the projected receiver positions. Profile and station numbers mentioned in the text are labelled.

Table 1. List of seismic refraction profiles. References for acquisition parameters: 1, Jokat *et al.* (1996); 2, Jokat *et al.* (1995). References for velocity models: 3, Mandler & Jokat (1998); 4, Schlindwein & Jokat (1999).

Profile	Number	Length (km)	Ref.
Gåsefjord	AWI-90300/310	235	1, 3
Gåsefjord	AWI-94400	270	2, 4
Fønfjord	AWI-90320	210	1, 3
Nordvestfjord	AWI-90380	220	1, 3
Nordvestfjord	AWI-94410	270	2
Kejser F. J. Fjord	AWI-94320	375	2, 4
Kong Oscar Fjord	AWI-94340	350	2, 4
Dickson Fjord	AWI-94360	230	2, 4

observed picks is shown to allow a qualitative estimation of model reliability. Out of 3984 picks in total for all considered *P* waves 98 per cent were matched by rays, and 96 per cent of all 3832 *S*-wave traveltime arrivals could be used to constrain the models. Errors in seismic velocities and depths of layer boundaries were estimated by perturbation of single node parameters until the fit of calculated traveltimes was no longer acceptable. The velocity uncertainties are hereby estimated as ± 0.1 km s^{-1} in the upper crust, and in the middle and lower crust and the upper mantle as ± 0.2 km s^{-1}. Errors in layer boundary depths depend on the number of reflected rays and vary between ± 1.0 and ± 2.0 km.

2.2 Nordvestfjord profile

The 270 km long profile of Nordvestfjord runs from northwest to southeast along the Nordvestfjord and northern part of Hall Bredning and ends with three stations on the sedimentary Jameson Land Basin (Fig. 2). The first 220 km long line was shot in the year 1990 (AWI-90380) and modelled by Mandler & Jokat (1998). In 1994, the transect was extended by 50 km towards the northwest (AWI-94410) with four new stations and the seismic source energy was doubled in comparison to the 1990 experiment. The additional stations (414–411) were modelled for the first time in this study to better image the increase of crustal thickness in this area. Fig. 3 shows, as an example, the eastern part of the seismic section of station 382. The rough seafloor topography of the deep Nordvestfjord, with only a negligible sedimentary cover, is reflected in pronounced undulations of the refracted crustal *Pg* phase. This can be observed at all western stations (414–386, Fig. 4). The records of the three stations on Jameson Land (387–389) contain only few diving waves through the sediments, so the detailed work of Fechner & Jokat (1996) and the seismic velocities obtained for the eastern part of the Gåsefjord

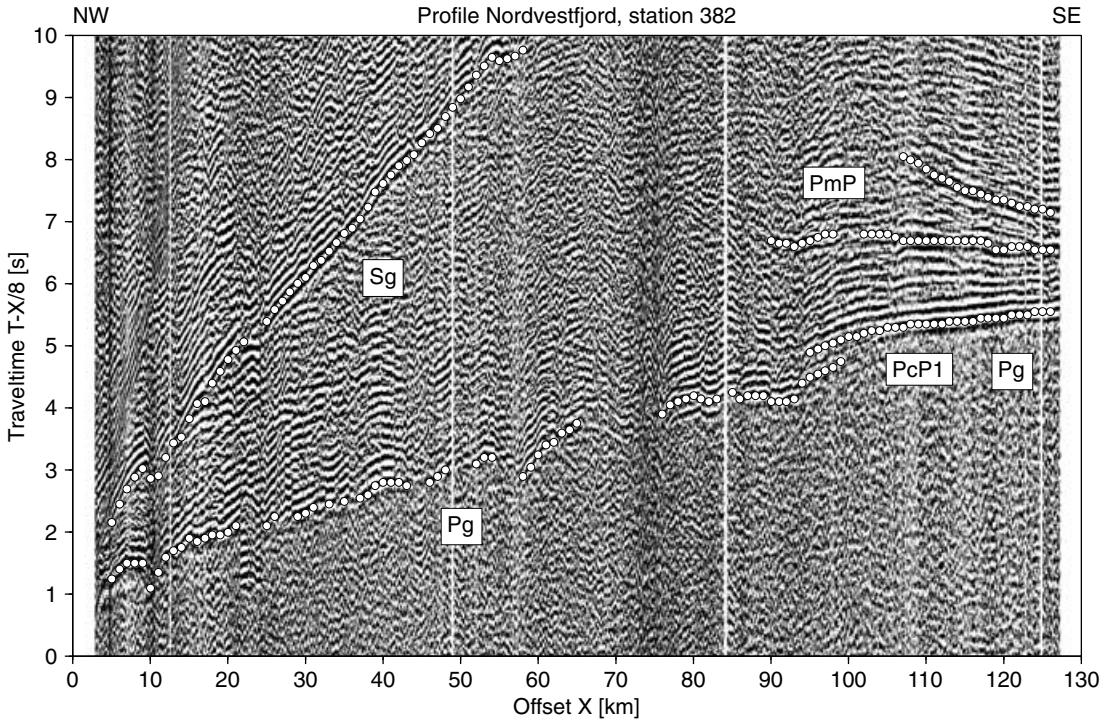

Figure 3. Example of a seismic record section from the Nordvestfjord profile (AWI-90380 and AWI-94410), station 382. Bandpass frequency filtering (3–17 Hz) and automatic gain control scaling (2000 ms) was applied. White dots show observed traveltime arrivals, the corresponding phases are labelled. Note the two branches of the *PmP* traveltime curves.

and Fønfjord (see next sections) profiles were used to represent the basin.

The upper crystalline crust is well covered by rays and clear *PcP*1 reflections are visible on several stations (e.g. station 382, Fig. 3 and station 414, Fig. 5), bounding the transition to the middle crust at 20–13 km depth (Fig. 6). In the area of the Caledonian fold belt, which also lacks a sedimentary cover, the seismic velocity increases rapidly from 5.6 km s^{-1} near the surface to 6.1 km s^{-1} at 4 km depth (Fig. 7). Underneath, the velocity increases more slowly to 6.4 km s^{-1} above the first crustal reflector, and to 6.7 km s^{-1} near the second crustal reflector along the entire profile. The second reflector is constrained by few *PcP*2 reflections and is located nearly parallel to the upper reflector at 30–20 km depth. At the crustal reflectors, a seismic velocity change of 0.05–0.2 km s^{-1} was modelled. The large velocity contrast between the upper and the middle crust at km 145–220 of the profile is reflected in strong *PcP*1 phases at the stations 382 and 383.

No diving waves determine the seismic velocity in the lower crust, so a constant gradient with a maximum of 6.9 km s^{-1} at the crust–mantle boundary (Moho) similar to the three transects of the northern Fjord Region was assumed (Schlindwein & Jokat 1999). The Moho topography is fairly complex but well sampled by rays. *PmP* reflections with reduced traveltimes of more than 9 s, recorded at the westernmost stations 414 (Fig. 5) and 413, result in a Moho depth as great as 48 km. East of the Caledonian orogen, the Moho rises up to 23 km beneath the Jameson Land Basin. Two branches of the *PmP* phases at stations 383 and 382 (Fig. 3) were used to model a Moho plateau at km 170 of the profile. On this transect, missing refracted *Pn* phases prevent the modelling of upper mantle velocities. Therefore, the velocity of 8.0 km s^{-1} derived from the nearby Gåsefjord and Fønfjord profiles (see next sections) was also used here.

The main difference from the previous *P*-wave model of Mandler & Jokat (1998) is the velocity gradient from the surface to the Moho. The former model contains fairly high seismic velocities in the upper and middle crust with values up to 6.6 km s^{-1} at 11–15 km depth and 6.8 km s^{-1} at 23–25 km depth. Since the newly incorporated stations (414–411, see also Fig. 5) gave clear evidence for much lower velocities, we modelled only 6.3 and 6.6 km s^{-1}, respectively, at these depths. Despite the higher crustal velocities of 6.4–7.1 km s^{-1}, Mandler & Jokat (1998) derived very similar Moho depths (23–30 km) compared with the new model for the easternmost part of the profile. This is mainly due to the different slope of the crust–mantle boundary in the models in this area. The large value for Moho depth (48 km) at the western end of our new model, although we used relatively low seismic velocities, is also a result of the inclusion of the new stations into the model.

2.3 Gåsefjord profile

The southwest–northeast trending Gåsefjord transect, which runs for 270 km along the Gåsefjord, Hall Bredning and Jameson Land (Fig. 2), was also acquired in 1990 (AWI-90300/310) and modelled by Mandler & Jokat (1998). It was extended in 1994 (AWI-94400) by two stations to the west and two stations in the Scoresby Sund and the model was modified by Schlindwein & Jokat (1999). Similar to the Nordvestfjord profile, Mandler & Jokat (1998) modelled much higher seismic velocities in the upper and middle crust than Schlindwein & Jokat (1999), who included new velocity information about the middle crust from the new western station 405 of the profile extension. To obtain consistent velocity models in the entire Fjord Region, we slightly revised the model of Schlindwein & Jokat (1999). An example seismic section (station 301) is shown in Fig. 8. Besides the undulating *Pg* diving phases from the upper

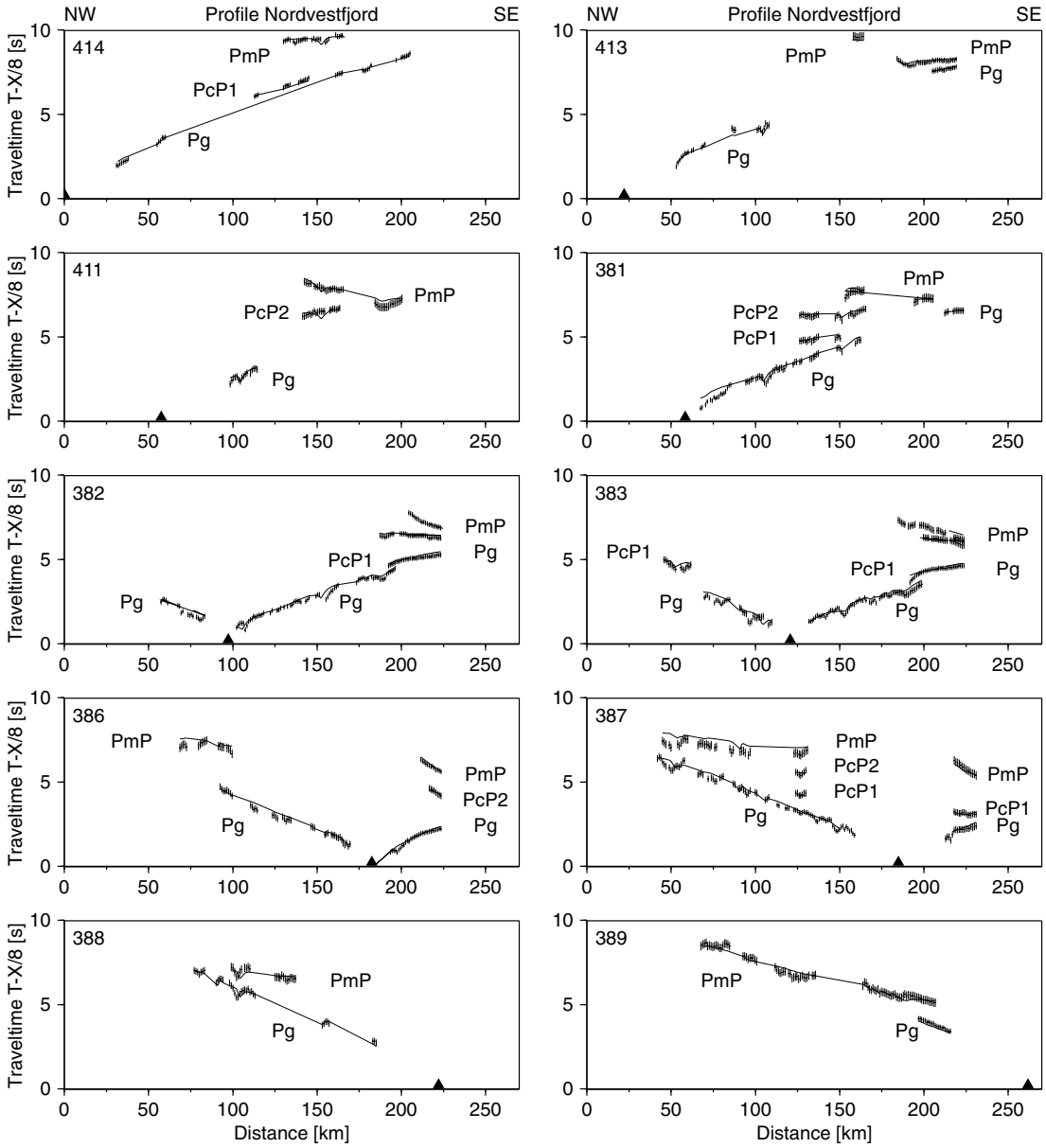

Figure 4. Observed and calculated *P*-wave arrivals for the Nordvestfjord profile (AWI-90380 and AWI-94410). Triangles show the locations of the receiver stations. Vertical error bars represent the observed arrivals and assigned errors; the solid lines denote the traveltime curves calculated from the velocity model. Station numbers and phases are labelled.

and middle crust, three crustal reflections (*PcP*1, *PcP*2 and *PcP*3) and two branches of the *PmP* traveltime curves are visible.

Refracted *Pg* arrivals could be found at each station (Fig. 9), so the upper crust is well covered by rays (Fig. 10). Several stations on Jameson Land (316–325), and the two ocean bottom hydrophones (401 and 402), helped to refine the seismic velocities of the two lower sedimentary layers (4.1–4.3 km s^{-1} and 5.6–5.8 km s^{-1}). Clear *Pn* phases on the three easternmost stations (323–325) lead to a modelled upper mantle velocity of 8.0 km s^{-1}. The velocity distribution of the crystalline crust is now similar to that in the Nordvestfjord profile and the previous model of Schlindwein & Jokat (1999), except for slightly higher (0.05–0.2 km s^{-1}) values in the upper crust and in the upper mantle (Fig. 11). The westernmost station, 405, shows a long *Pg* branch, which yields seismic velocities for the middle crust. This part of the crust is divided by three reflectors that are constrained by several stations. The first two reflectors are almost horizontal at depths of about 13 and 20 km. The lowermost reflector appears at a depth of 37 km at the western end of the transect and rises continuously up to 21 km beneath Jameson Land. Again, a seismic velocity contrast of 0.05–0.2 km s^{-1} was modelled at the two lower reflectors.

There have been differing interpretations of the branched *PmP* reflections on the stations 301 and 302 which have occurred during observations by various authors. Mandler & Jokat (1998) modelled them as reflections from the upper and lower boundary of a thin, high-velocity layer (7.3 km s^{-1}), interpreted as magmatic underplating, but Schlindwein & Jokat (1999) considered them partly as crustal reflections and questioned the existence of an underplated body in the Scoresby Sund region. Similar to the Nordvestfjord profile, we preferred to model the two branches of the

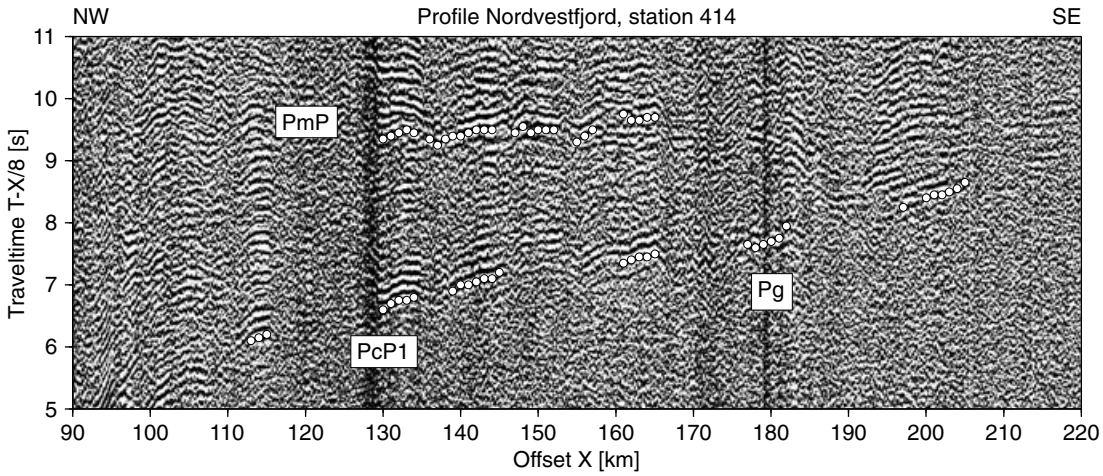

Figure 5. Example of a seismic record section from the Nordvestfjord profile (AWI-90380 and AWI-94410), station 414. For additional explanations see Fig. 3.

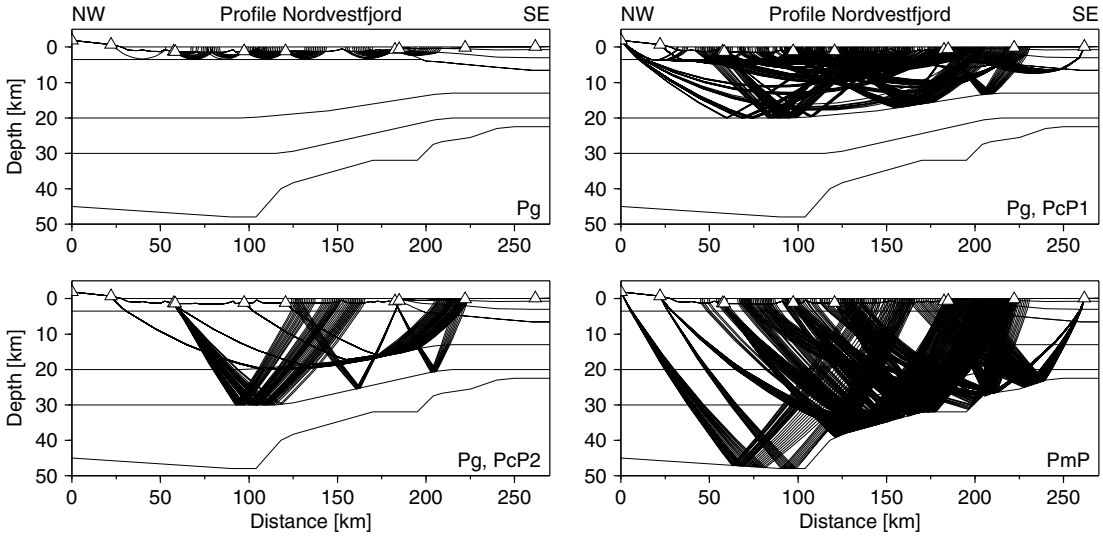

Figure 6. Ray tracing of *P* waves for the Nordvestfjord profile (AWI-90380 and AWI-94410). For each layer, the coverage with refracted and reflected rays traced to observed picks is shown. The corresponding phases are labelled. Triangles mark the receiver locations. The vertical exaggeration is ×2.

traveltime curves as a result of pronounced Moho topography rather than as the result of magmatic underplating. This interpretation is also supported by the finite-difference modelling, which will be discussed later. The depth of the Moho ranges from 44 km below the Caledonides to 21 km at the eastern end of the transect beneath Jameson Land. These depths are well below the values derived by Mandler & Jokat (1998) (22–49 km) but they are akin to those in the model of Schlindwein & Jokat (1999). Only the new Moho slope includes a plateau at km 110–140 necessary to explain the reflected phases.

2.4 Fønfjord profile

The 210 km long Fønfjord profile was shot in 1990 (AWI-90320) and first modelled by Mandler & Jokat (1998). It runs in a west–east direction close to the Gåsefjord profile (Fig. 2). The two transects show very similar distribution of seismic velocities with 5.6 km s^{-1} at the surface and 6.9 km s^{-1} above the crust–mantle boundary, the upper mantle velocity is also 8.0 km s^{-1}. The crust is divided by three reflectors at 13, 20 and 28–21 km depth with velocity changes of 0.05–0.1 km s^{-1} (Fig. 12). Differences occur in the Moho topography. The maximum depth of the modelled crust–mantle boundary in this profile is only 38 km in the western half of the transect, and after km 100 of the profile it rises steeply to 21 km underneath Jameson Land, where it merges with the lowermost crustal reflector, as seen modelled in the Gåsefjord profile. In comparison with the model of Mandler & Jokat (1998), two main differences should be noted: First, as in all other transects, much lower seismic velocities were modelled in this study. Second, no evidence for a high-velocity layer in the lower crust was found in the model, instead two *PmP* branches that occur at the two westernmost stations, 321 and 322, are explained by shape of the Moho.

2.5 Poisson's ratio

For all six profiles shown in Fig. 2 shear wave modelling was performed. We converted the *P*-wave velocity models to *S*-wave velocity models assuming a Poisson's ratio of 0.25 as a starting model.

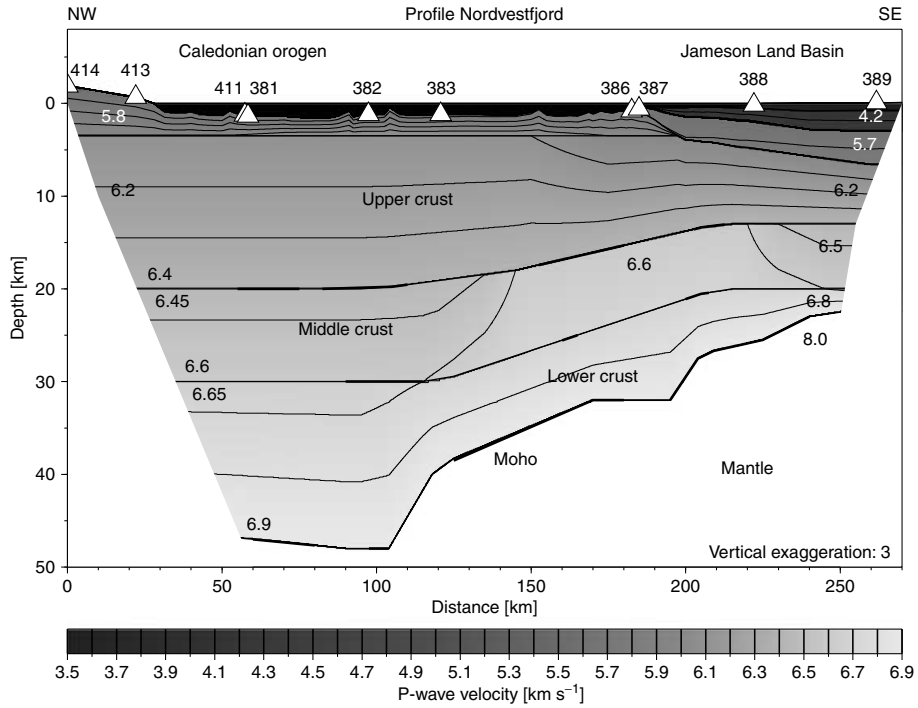

Figure 7. *P*-wave velocity model for the Nordvestfjord profile (AWI-90380 and AWI-94410). Contour interval is 0.1 km s^{-1}. Some velocity values (in km s^{-1}) are noted. Triangles mark the locations of the receiver stations. Some stations are labelled. Bold lines represent the parts of the layer boundaries constrained by reflected waves. The vertical exaggeration is ×3.

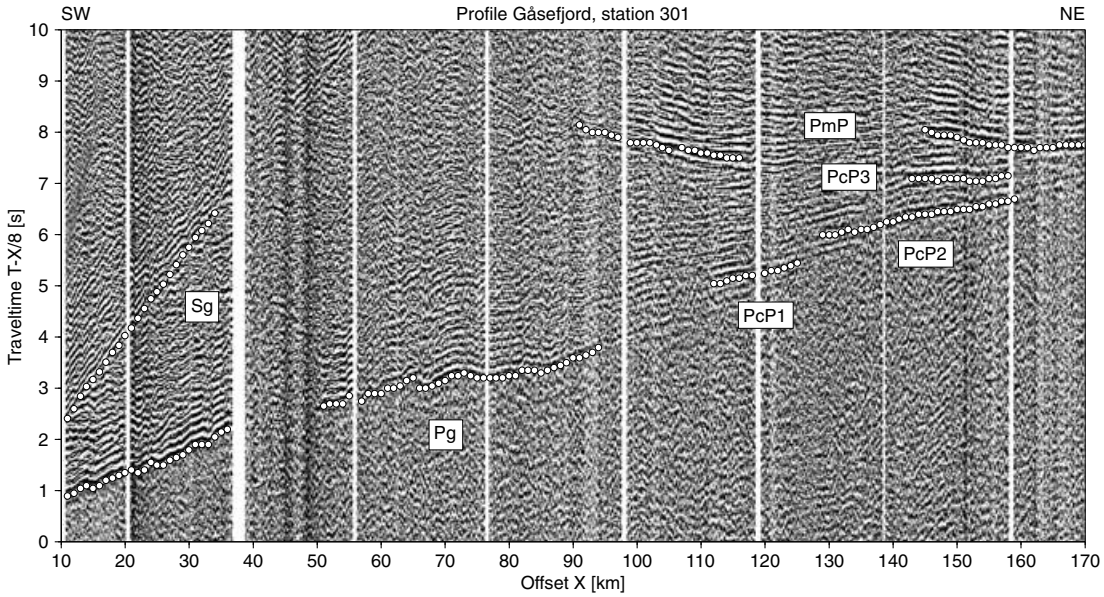

Figure 8. Example of a seismic record section from the Gåsefjord profile (AWI-90300/310 and 94400), station 301. Note the two branches of the *PmP* traveltime curves. For additional explanations see Fig. 3.

For the three northern transects, the *P*-wave velocity models after Schlindwein & Jokat (1999) were used. We then refined the models with ray tracing of observed shear wave arrivals on 51 seismic record sections (Fig. 13). In the refinement process, the layer boundaries were kept fixed and only velocity variations were applied. The quality of *S*-wave arrival data in the sedimentary basins is poor, so there are few constraints on the *S*-wave velocity structure. However, a sufficient number of refracted *Sg* arrivals allowed direct modelling of the upper crystalline crust (Fig. 14). The middle and lower crust could only be modelled indirectly using some reflected phases, mostly *SmS*, so the resolution on details here is also poor. *Sn* phases are missing on almost all stations, only one short traveltime branch of 15 km offset was found (Fig. 13, Dickson Fjord profile). This allowed no *S*-wave velocity model of the upper mantle. Shear wave velocities in the crystalline crust range between 3.2 and 3.6 km s^{-1} in the upper crust, 3.5 and 3.9 km s^{-1} in the middle crust and 3.8 and 4.0 km s^{-1} in the lower crust; the high-velocity body of the northern profiles shows values up to 4.2 km s^{-1}.

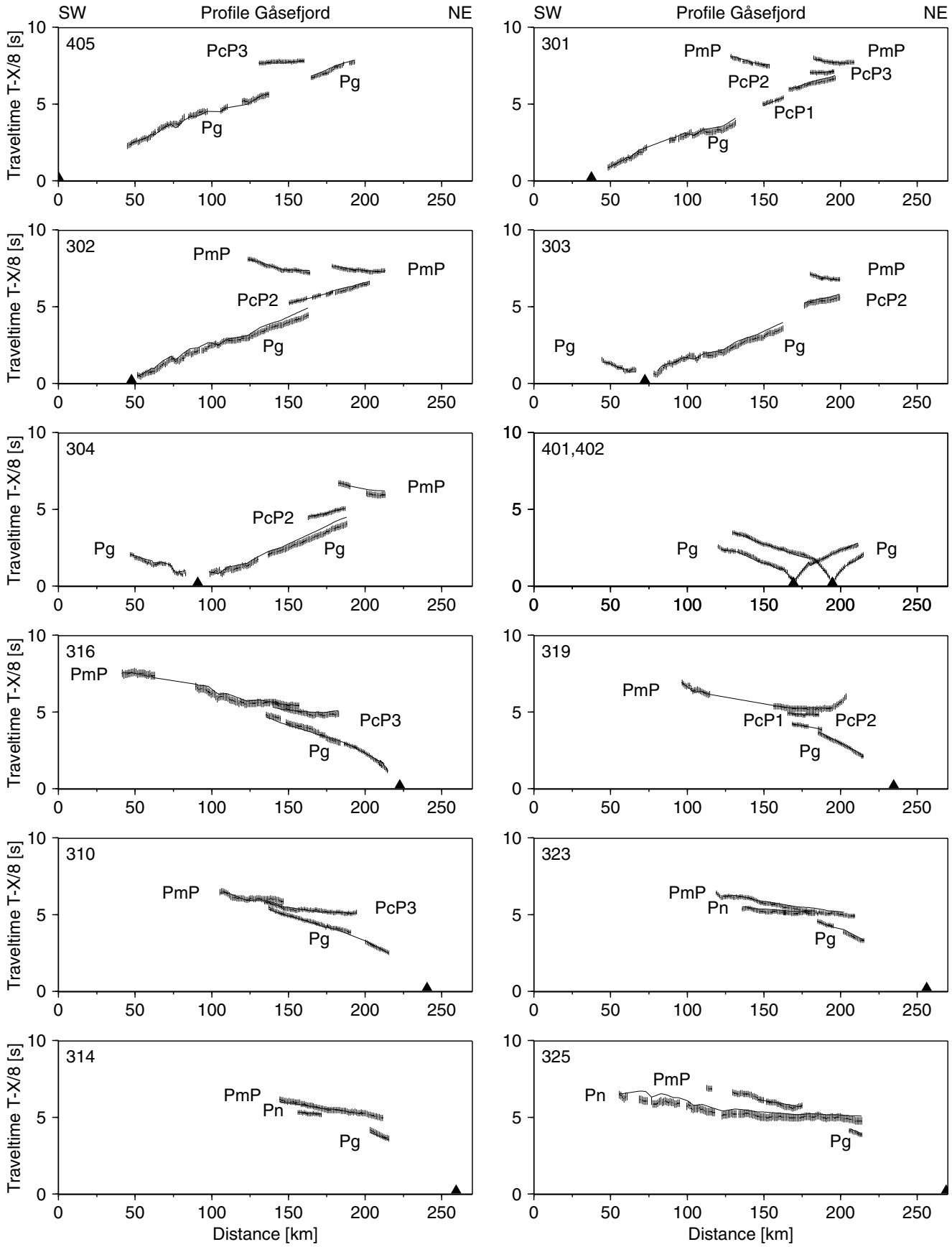

Figure 9. Observed and calculated *P*-wave arrivals for the Gåsefjord profile (AWI-90300/310 and 94400). For additional explanations see Fig. 4.

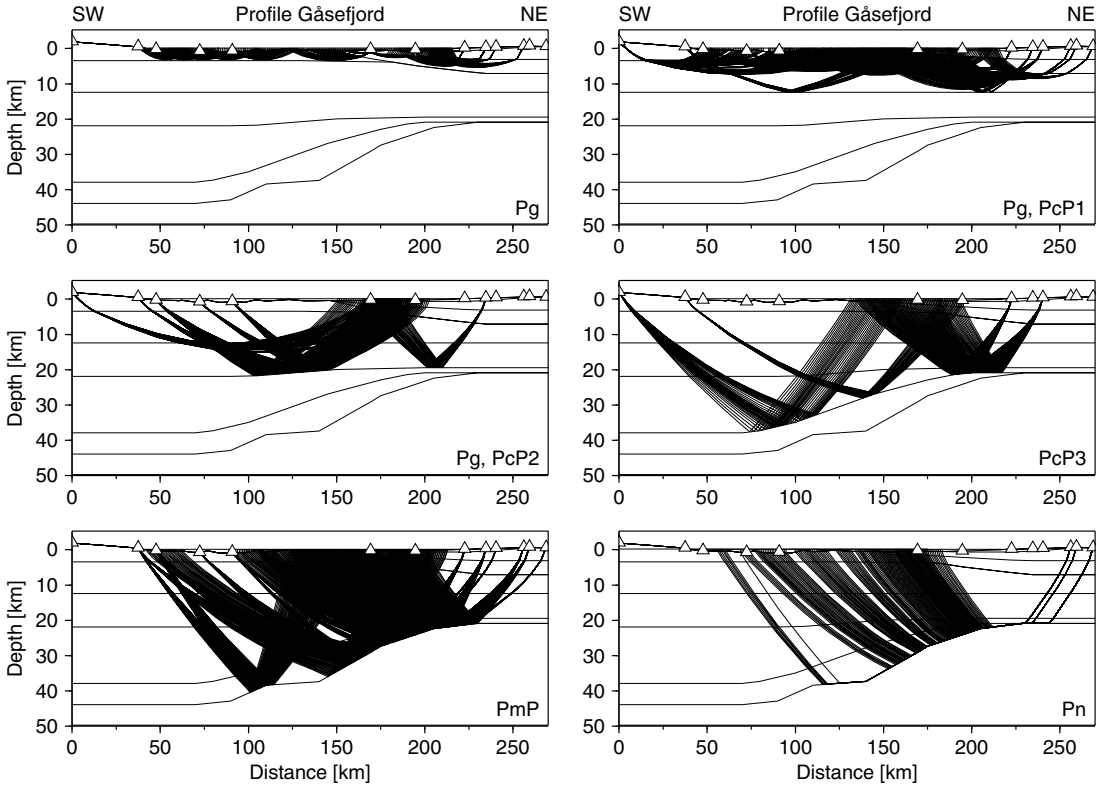

Figure 10. Ray tracing of *P* waves for the Gåsefjord profile (AWI-90300/310 and 94400). For additional explanations see Fig. 6.

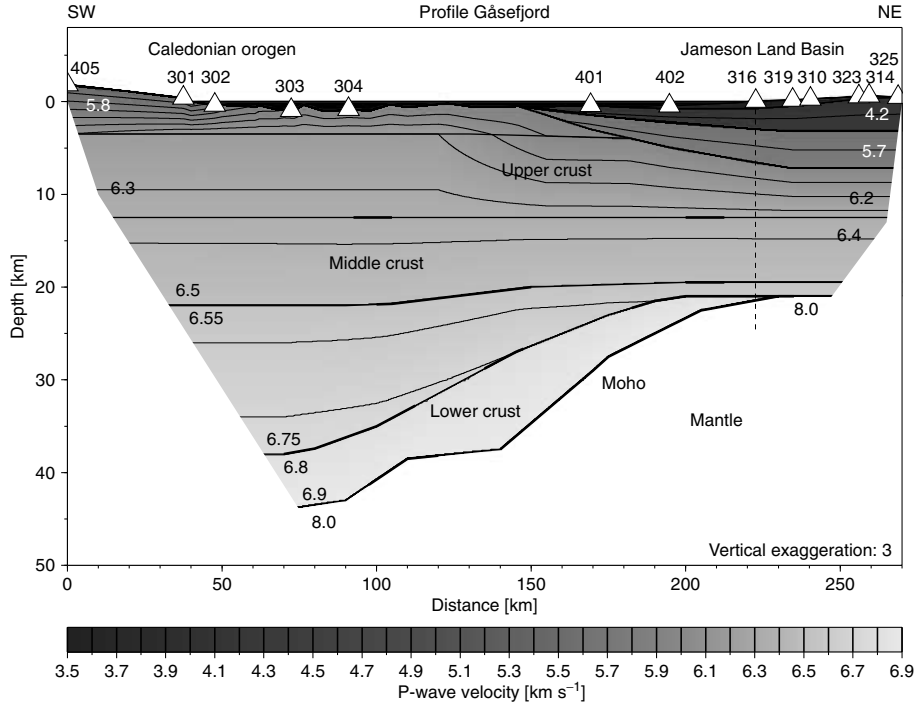

Figure 11. *P*-wave velocity model for the Gåsefjord profile (AWI-90300/310 and 94400). The dashed line indicates the intersection with the Fønfjord profile (AWI-90320). For additional explanations see Fig. 7.

Poisson's ratio was calculated for all profiles in order to compare the models of *P*- and *S*-wave velocities (Fig. 15). The three models of the northern Fjord Region (Kejser Franz Joseph Fjord, Kong Oscar Fjord and Dickson Fjord profiles) show small areas with a Poisson's ratio higher than the initial value of 0.25, reaching values of up to 0.30 in the uppermost crystalline crust (Kejser Franz Joseph Fjord profile). Two models (Nordvestfjord and Dickson Fjord profiles) show slightly reduced Poisson's ratios between 0.23 and 0.24 in the

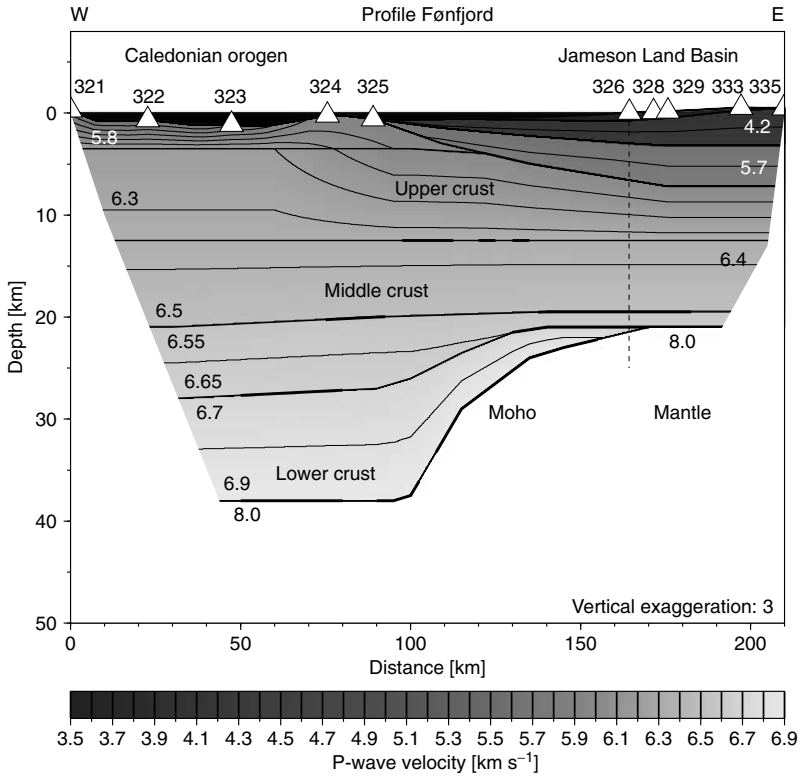

Figure 12. *P*-wave velocity model for the Fønfjord profile (AWI-90320). The dashed line indicates the intersection with the Gåsefjord profile (AWI-90300/310 and 94400). For additional explanations see Fig. 7.

upper crust. In the middle crust, most models contain lower values down to 0.22. With the exception of a small region in the Dickson Fjord profile no lateral variations of Poisson's ratio are observed in the lower crust.

3 FINITE-DIFFERENCE MODELLING

The newly derived models of the southern Fjord Region suggest no magmatic underplating beneath the lower crust, in contrast to the work of Mandler & Jokat (1998) who cited results of their first-order amplitude modelling in support of underplating. Instead, the key *PmP* arrivals of the western stations (301–302, Gåsefjord profile, and 321–322, Fønfjord profile) are modelled by a pronounced Moho topography. Schlindwein & Jokat (1999), who presented models without underplating, conducted no amplitude modelling at all. As the ray tracing modelling yielded no preference for either of these models, a comprehensive 2-D finite-difference amplitude model was constructed.

3.1 Modelling technique

In contrast to the ray tracing technique, which uses a high-frequency approximation of the wave equation, the finite-difference (FD) method calculates the complete wavefield. Numerical approximations are done by the discretization of the model on a rectangular grid with equidistant nodes and by using equally spaced discrete time steps. The partial derivations of the wave equations are replaced by differential operators. The FD method uses not only velocity contrasts at layer boundaries but also the complete acoustic impedance, and calculates *P* and *S* waves and all converted phases. Therefore, FD modelling allows an extensive analysis of wave amplitudes, especially of reflected phases.

We used the FDVEPS program (Bohlen 2002), which calculates wave fields in inhomogeneous viscoelastic media. As our medium is considered to be fully elastic, only the seismic velocities for *P* and *S* waves and the density are required. The seismic velocities are well known from the 2-D ray tracing modelling and the density of the crystalline crust was calculated after Christensen & Mooney (1995). The water layer and the upper two sedimentary layers of the Jameson Land Basin were replaced by one layer with seismic velocities of 4.5 and 2.6 km s^{-1} respectively. Using these higher velocities allowed us to reduce the distance between two gridpoints significantly, leading to a substantial saving of working memory. In doing so, errors in traveltimes do not exceed 180 ms, which can be accepted as traveltimes were modelled much more accurately with ray tracing. To keep the computing time short, a Ricker wavelet with a centre frequency of 5 Hz was chosen for the source signal. For the following considerations, there is no advantage in using the real signal, which contains frequencies up to 17 Hz, because only the amplitude, and not the shape, of the wavelet is important. Due to the fully elastic modelling, where no damping is applied, the modelled amplitude of the wavelet is independent of its frequency. It is influenced only by spherical divergence and the reflection coefficients.

3.2 Amplitude analysis

Fig. 16 shows the result of the modelling of station 302, one of the western stations in the Gåsefjord profile (Fig. 11), which contains two *PmP* branches with high apparent velocities. The synthetic seismogram clearly shows the existence of three reflected *PmP* phases, with traveltimes curves covering an offset range much larger than

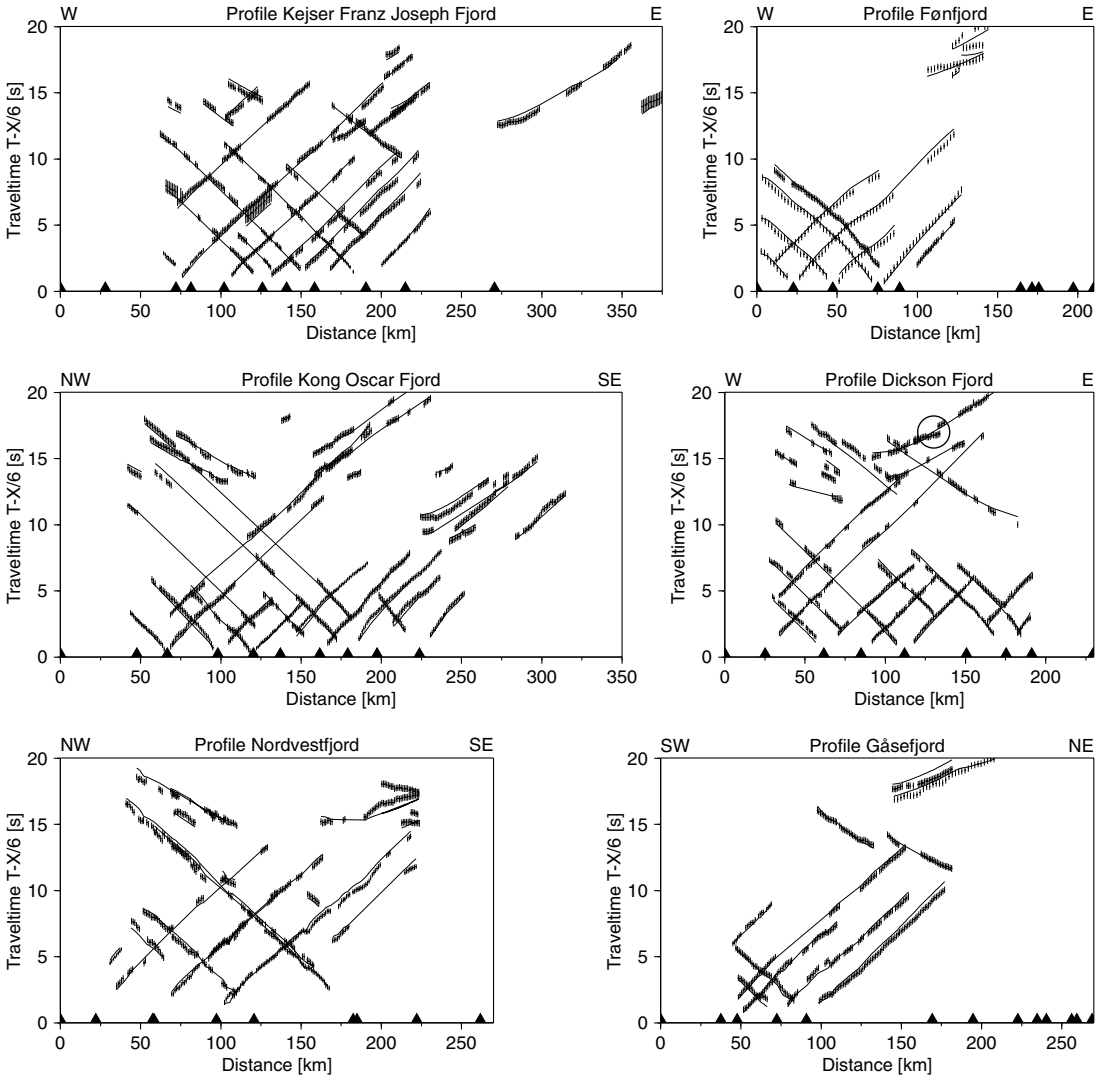

Figure 13. Observed and calculated *S*-wave arrivals for all profiles. Triangles show the locations of the receiver stations. Vertical error bars represent the observed arrivals and assigned errors; the solid lines denote the traveltime curves calculated from the velocity model. The black circle (Dickson Fjord profile) marks the *Sn* phase.

could be observed. Similar results were derived from the FD modelling of the stations 301 (Gåsefjord profile), 321 and 322 (Fønfjord profile) and 382 and 383 (Nordvestfjord profile). Thus, the occurrence of branched Moho reflections can indeed be explained by pronounced Moho topography. Unfortunately, the offset range of the observed reflections is too short for amplitude considerations. Instead, station 316 (Gåsefjord profile) was used for amplitude modelling because it is the only station which reveals a pronounced *PmP* phase of sufficient quality over a large offset (about 70 km). The real and synthetic seismograms, using the newly derived velocity model (Fig. 11) are shown in Fig. 17. As the lower crust is very thin beneath this station, the *PcP*3 crustal reflection and the *PmP* phase are close to one another. At offsets smaller than 60 km the *PmP* phase shows a pronounced delay relative to the predicted traveltimes, which might be an effect of a 3-D Moho topography. Therefore, this part was excluded from the following amplitude considerations.

For station 316, synthetic seismograms of several models, which differ in particular in the lower crust, were calculated to test the likelihood of an underplated body (Fig. 18). Next, the amplitudes of the modelled *PmP* phases were picked and compared with the real data (Fig. 19). The first arrivals of the *PmP* reflection were difficult to determine in the real seismogram without automatic gain control scaling due to the high noise level. Therefore, a 500 ms wide strip encompassing the assumed first arrivals of the *PmP* was cut out of the data and filtered with a 5 km long median filter to reduce the influence of noise. The amplitudes show a steep increase until an offset of about 85 km, where a maximum is reached, followed by a nearly symmetric decrease until an offset of 100 km whereafter the amplitudes remain on a low level (Fig. 19a).

The first model, 1, is the newly derived model (Figs 11 and 18), whose amplitude characteristics fit the real data very well (Fig. 19b). To test the influence of the acoustic impedance at the crust–mantle boundary, a modified model, 1A, with high velocities in the lower crust, was calculated (Fig. 18). There is only a small difference from the amplitudes of model 1 (Fig. 19b). This must be the result of the slightly different acoustic impedance (change of 3 per cent), because the topography of the Moho remained the same. The second model, 2 (Fig. 18; Schlindwein & Jokat 1999), shows a similar amplitude distribution to models 1 and 1A, except for a minor displacement of the maximum (Fig. 19c). This is mainly due to the different Moho

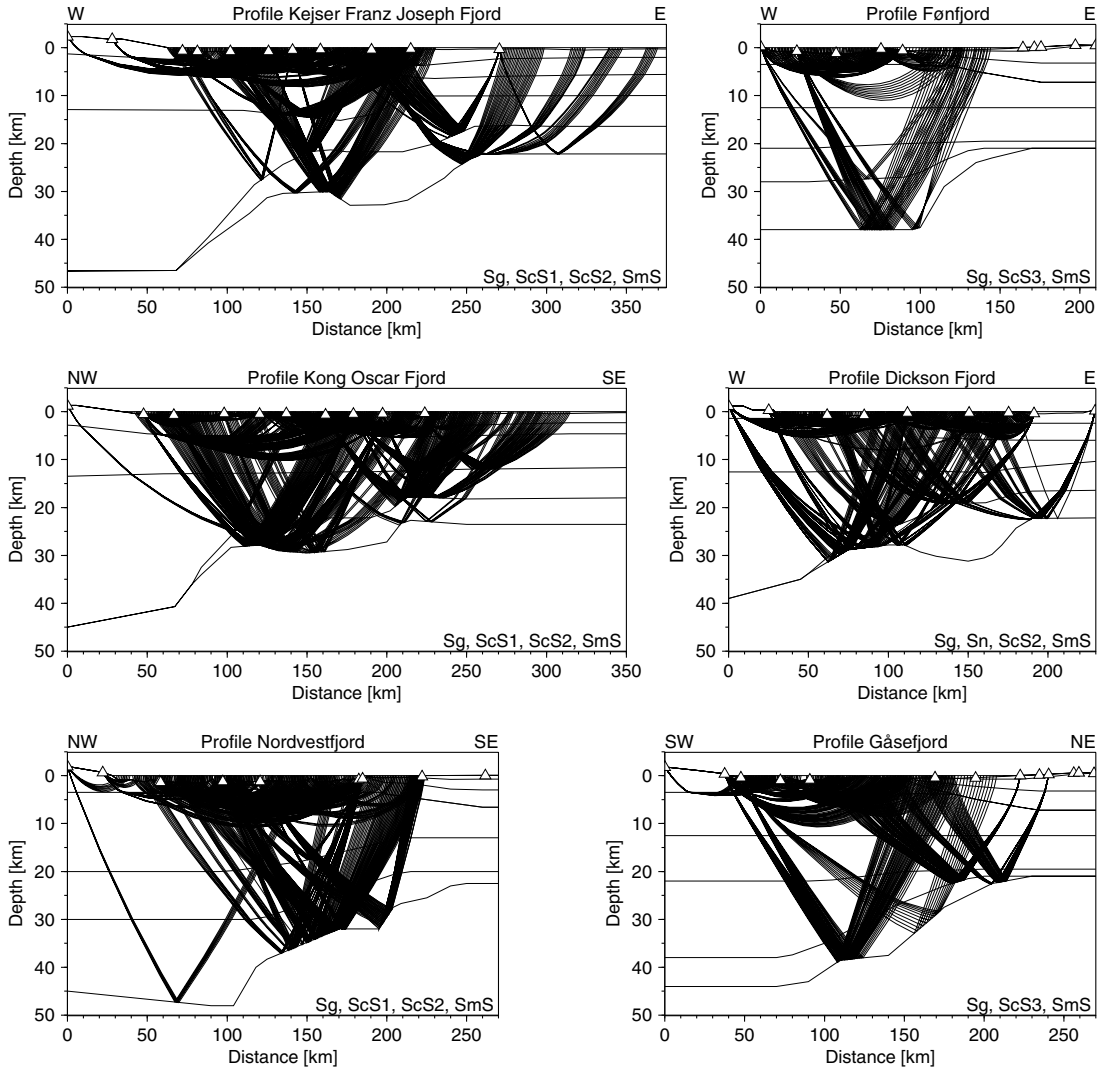

Figure 14. Ray tracing of *S* waves for all profiles. For all layers, the coverage with refracted and reflected rays traced to observed picks is shown. The corresponding phases are labelled. Triangles mark the receiver locations. Vertical exaggeration is ×3.

slope, as the deviating mantle velocity of 7.94 km s^{-1} changes the acoustic impedance less than 1 per cent. A completely different amplitude behaviour occurs for model 3 (Fig. 18; Mandler & Jokat 1998). Here, until an offset of 100 km, the amplitudes are very low, and the increase at larger offsets is much smoother than that observed in the data (Fig. 19d). The removal of the high-velocity layer in the lower crust (model 3A, Fig. 18), which again changes the acoustic impedance by about 3 per cent, yielded a similar amplitude curve (Fig. 19d).

Hence, the amplitudes of the *PmP* reflection are only slightly influenced by the acoustic impedance contrast between crust and mantle. This can clearly be seen in comparing models 1 and 1A or 3 and 3A, respectively. Therefore, consideration of acoustic impedance alone can yield no conclusion about the existence of a high-velocity layer. The topography of the Moho reflector is crucial for the amplitudes, as this influences the angles of incidence and reflection, and, consequently, the reflection coefficient and the amplitudes. This is proved by models 1A and 3A where the acoustic impedances are the same. The striking amplitude variations must therefore be the consequence of the different reflector slopes. A complex Moho shape is hence both necessary and sufficient to resolve the real data amplitudes, whereas a high-velocity layer in the lower crust is neither necessary nor sufficient. Moho topography alone can, hence, be responsible for observed traveltime branches too. Thus, a high-velocity layer in the lower crust, and its interpretation as a magmatic underplate, is unlikely in the southern Fjord Region.

4 TECTONIC CONSIDERATIONS

4.1 The Caledonian orogen

The newly modelled deep seismic transects over the Caledonian orogen resulted in seismic velocities of 5.5 km s^{-1} near the surface, 6.4 km s^{-1} at 15–20 km depth and a continuous increase in the middle and lower crust to 6.9 km s^{-1} at the crust–mantle boundary (30–48 km depth). These velocities are well within the range typical for Palaeozoic mountain belts (e.g. Meissner 1986; Christensen & Mooney 1995) and similar to the results for the northern Fjord Region (Schlindwein & Jokat 1999). Moho depths up to 48 km in the Nordvestfjord profile raise again the question concerning the existence of a crustal mountain root. Besides a crustal root, Mandler & Jokat (1998) discussed another possible explanation for

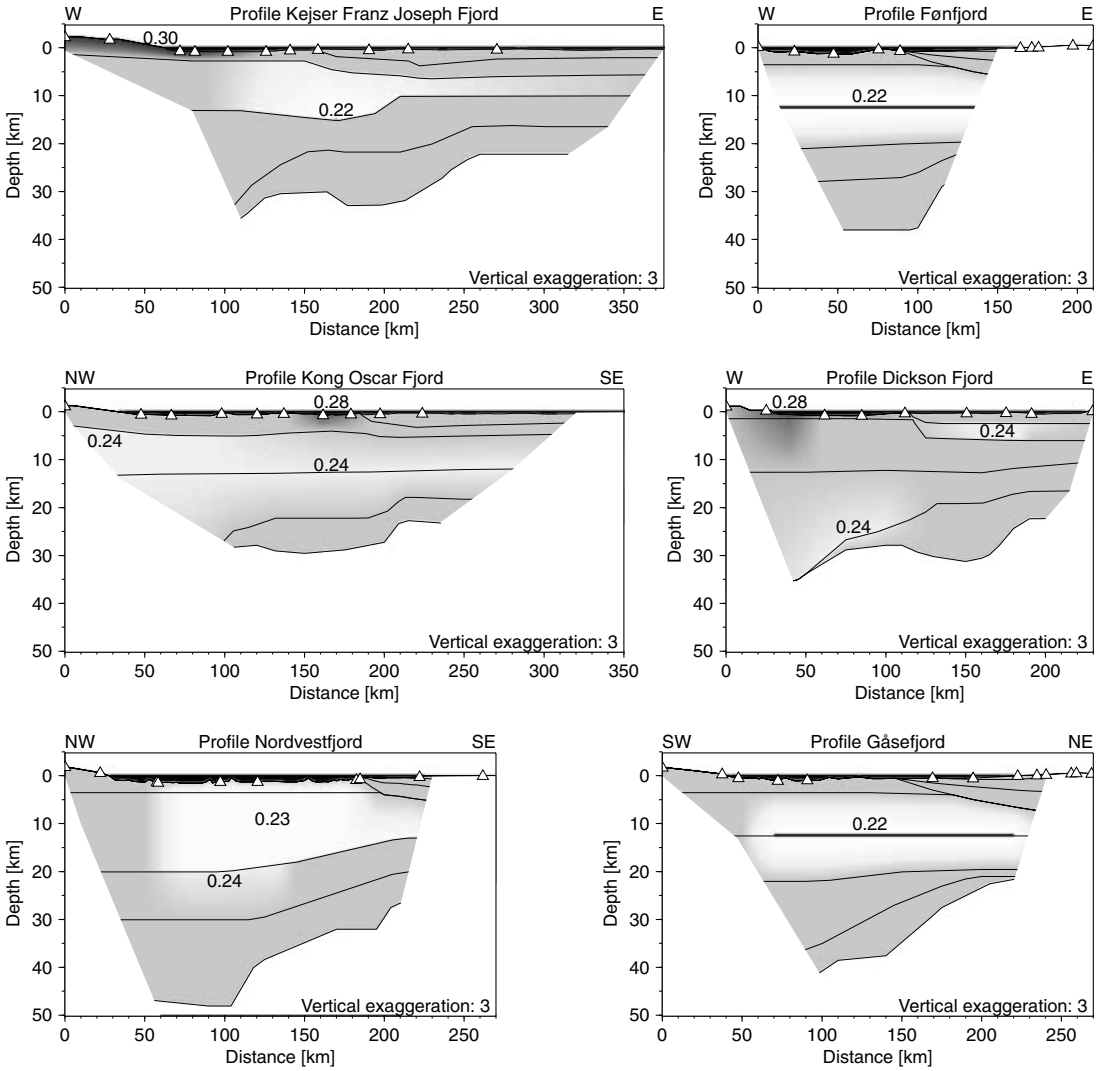

Figure 15. Model of Poisson's ratio for all profiles. Grey areas indicate no deviation from the initial value (0.25), bright regions show lower ratios and dark regions show higher ratios. Extreme values are annotated. Triangles mark the locations of the recording stations. Vertical exaggeration is ×3.

high crustal thicknesses in the region: the transition to the Precambrian shield of Central Greenland might result in large Moho depths, as shields can reach crustal thicknesses up to 50–55 km (e.g. Meissner 1986; Durrheim & Mooney 1994). But the observed thick crust is located in an area of the orogenic belt, where Caledonian foreland is exposed in only a few tectonic windows (Fig. 1), so we favour here the model of a crustal root. Additional gravity modelling supports this theory (Schmidt-Aursch & Jokat 2005).

Shear wave modelling of six profiles in the northern and southern Fjord Region, and calculation of Poisson's ratio yielded values between 0.22 and 0.30 in the upper and middle crust. Consideration of Poisson's ratio might support the interpretation of seismic velocity models. For example, in North America Musacchio *et al.* (1997) differentiated by means of Poisson's ratio the Precambrian Grenville Province (0.26–0.29) from the younger Appalachian Province (0.22–0.26) and derived additional information about the crustal composition. For the southern Urals, Carbonell *et al.* (1996) could assign Poisson's ratios of 0.22–0.31 to different rock types. For East Greenland, a clear distinction between the Caledonian fold belt and the adjacent rifted areas by means of variations in Poisson's ratio, which might be expected on the basis of changes in lithology, was not possible. Although the variations seen in the seismic transects are within the same range they are either very small and diverse, especially near the surface, or span both tectonic provinces equally, mostly in the middle crust. Neither are there any variations in Poisson's ratio within the Caledonides, which will allow us to expand a density model of the orogen constrained by seismic refraction data further to the west (Schmidt-Aursch & Jokat 2004).

4.2 The sedimentary basins

Extensional collapse of the Caledonian orogen in Devonian times, and the ensuing long-term rifting led to the formation of several sedimentary basins in the eastern realm of the Fjord Region (Fig. 1). The structure of the Jameson Land Basin was not remodelled in the seismic profiles, and instead we adopted the detailed results of Fechner & Jokat (1996) except with slightly adjusted seismic velocities (about 0.2 km s^{-1}) for the lower two sedimentary layers to fit the traveltime curves of single stations, especially the newly modelled ocean bottom hydrophones. Shear wave modelling and calculation of Poisson's ratio yielded no new insights due to a lack of *S*-wave phases on the seismic records of the eastern stations.

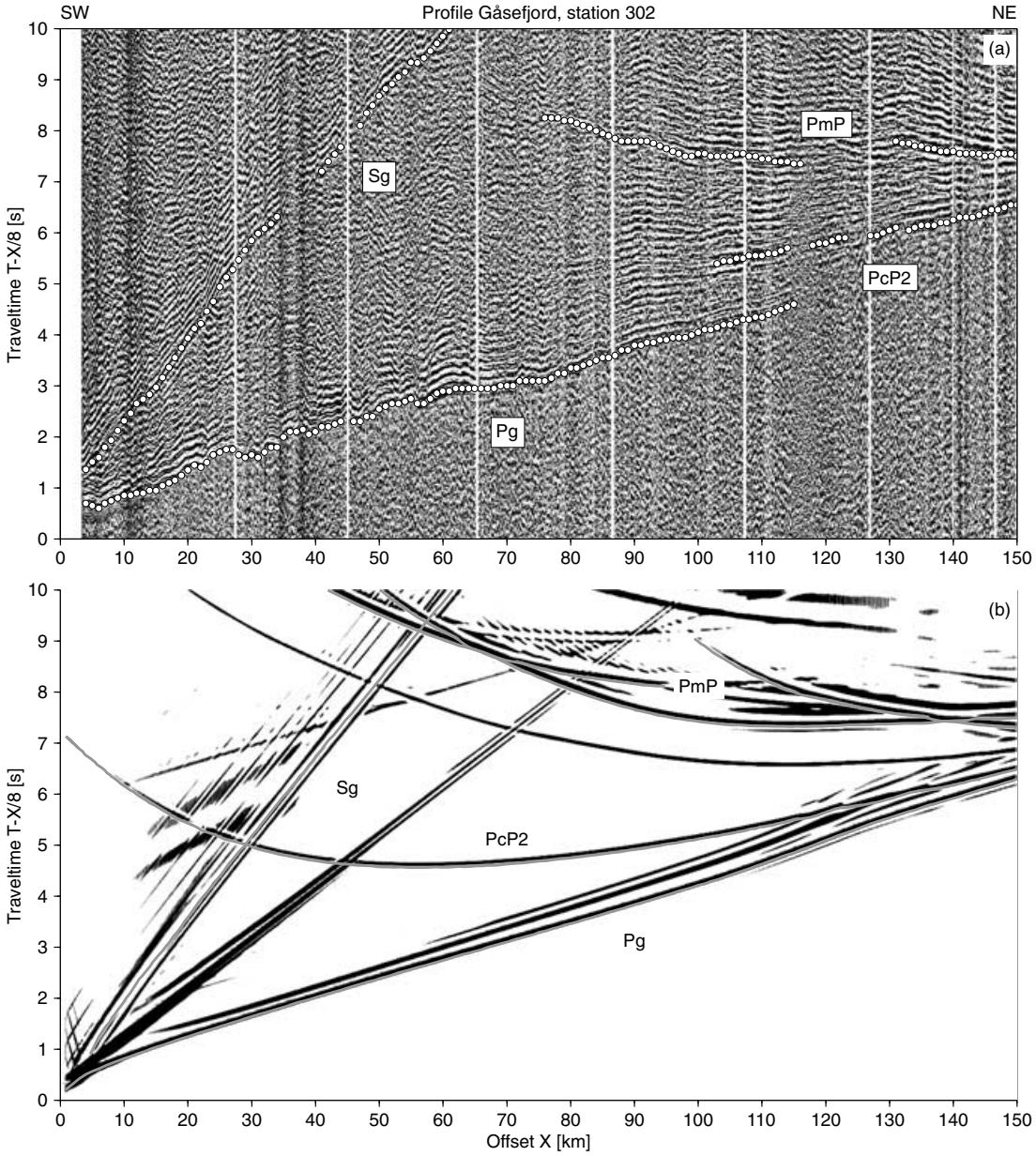

Figure 16. (a) Example of a seismic record section from the Gåsefjord profile (AWI-90300/310 and 94400), station 302. For additional explanations see Fig. 3. (b) Record section of the FD modelled synthetic seismogram. Trace normalization and bias was applied. Important phases are marked and labelled.

4.3 The Tertiary igneous province

The East Greenland Fjord Region belongs to the North Atlantic Igneous Province, which is related to the influence of the Icelandic hotspot in Tertiary times (see Saunders *et al.* 1997, for a review). Large amounts of flood basalts cover the area south of Scoresby Sund but only sparse extrusives occur north of 72°N (Fig. 1). The Jameson Land Basin was also covered by thick basalt sequences, which were completely eroded during uplift of the basin (Larsen & Marcussen 1992). Deep seismic profiles, combined with magnetic data, led to the conclusion that north of 72°N the majority of melts were trapped in the lower crust beneath the Mesozoic basins (Schlindwein & Jokat 1999). Magmatic underplating was discussed by Mandler & Jokat (1998) for the Scoresby Sund area, but additional data in conjunction with remodelling of the older deep seismic profiles, as well as finite-difference amplitude modelling, negate the existence of underplating in this area. This endorses the tectonic model of Schlindwein & Jokat (1999), which explains the different styles of magmatism in the northern (pronounced magmatic underplating in the lower crust, only minor extrusives) and southern (no underplating, large amounts of flood basalts) Fjord Region by the different rifting history of both areas.

5 CONCLUSIONS

We present a regional crustal model of central East Greenland between 69°N and 74°N. It covers the Caledonian fold belt and the rifted areas of the Fjord Region with the Devonian and Mesozoic basins. For this purpose, existing velocity models were inspected, expanded and, where necessary, modified. In the southern Fjord

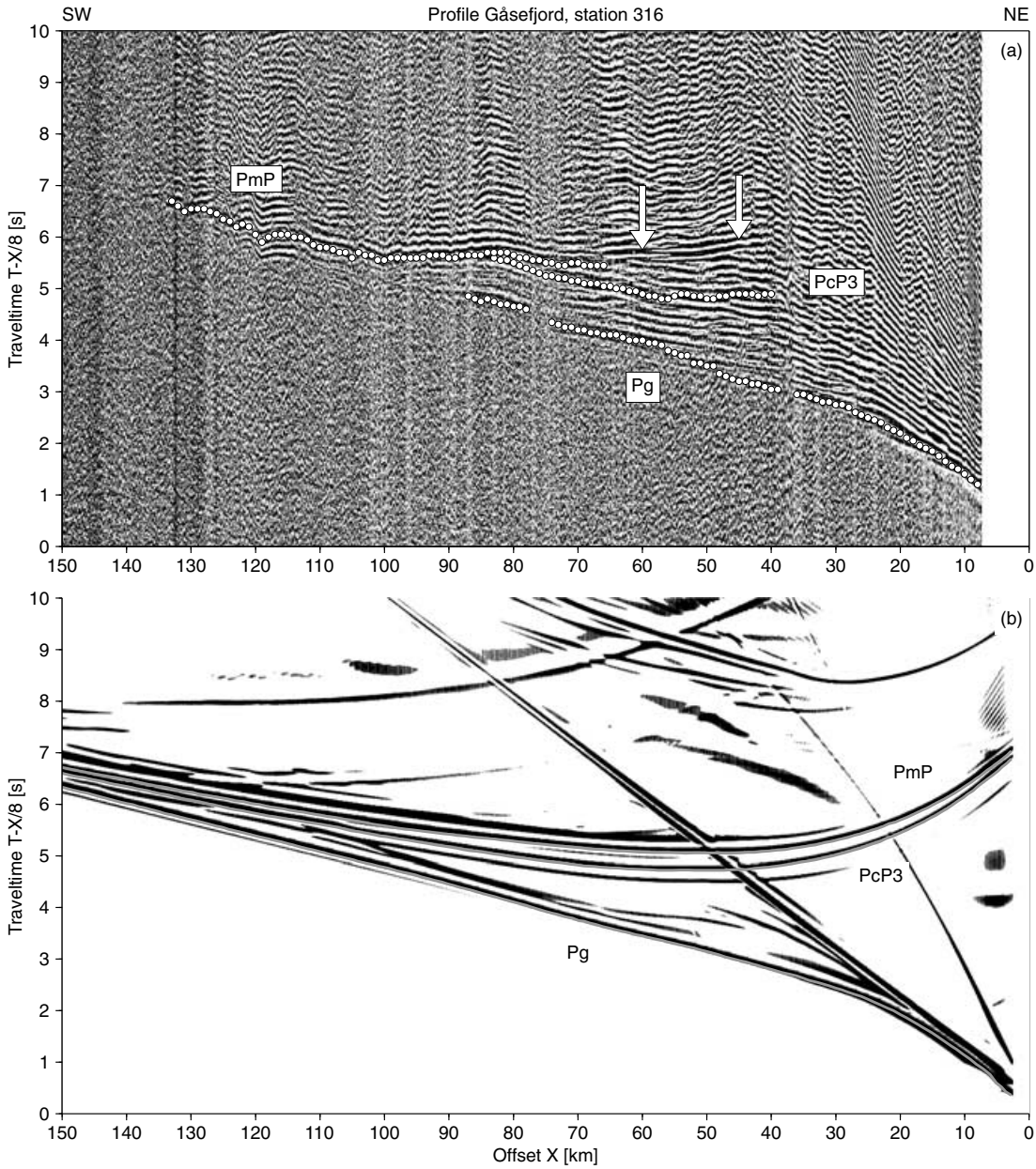

Figure 17. (a) Example of a seismic record section from the Gåsefjord profile (AWI-90300/310 and 94400), station 316. Arrows mark the part of the *PmP* phase which is excluded from the amplitude considerations. For additional explanations see Fig. 3. (b) Record section of the FD modelled synthetic seismogram (model A, Fig. 18). For additional explanations see Fig. 16(b).

Region, three remodelled and expanded refraction lines yielded consistent regional velocity models with seismic velocities between 5.5 km s^{-1} in the uppermost crust and 6.9 km s^{-1} above the crust–mantle boundary. These velocities are typical for regions of Precambrian and Palaeozoic age. One deep seismic line yielded Moho depths up to 48 km, indicating the existence of a crustal root beneath the Caledonian orogen.

Shear wave models were compiled and Poisson's ratio was calculated for all six seismic transects. Poisson's ratio shows large-scale variations between 0.22 and 0.24, mainly in the middle part of the crust. Small-scale variations in the crystalline upper crust, with values between 0.22 and 0.30, can be found in some profiles. These results will give additional constraints for further gravity modelling. Because ray tracing didn't yield a unique solution, finite-difference modelling was conducted to address the origin of Moho reflections in the Gåsefjord and Fønfjord profiles. Analysis of amplitudes from phases in different models enables us to conclude that a high-velocity layer, and thus magmatic underplating, is unlikely in the Scoresby Sund area.

ACKNOWLEDGMENTS

We thank the Geological Survey of Denmark and Greenland for the digital geological map of Greenland. The finite difference software was kindly provided by T. Bohlen. The manuscript greatly

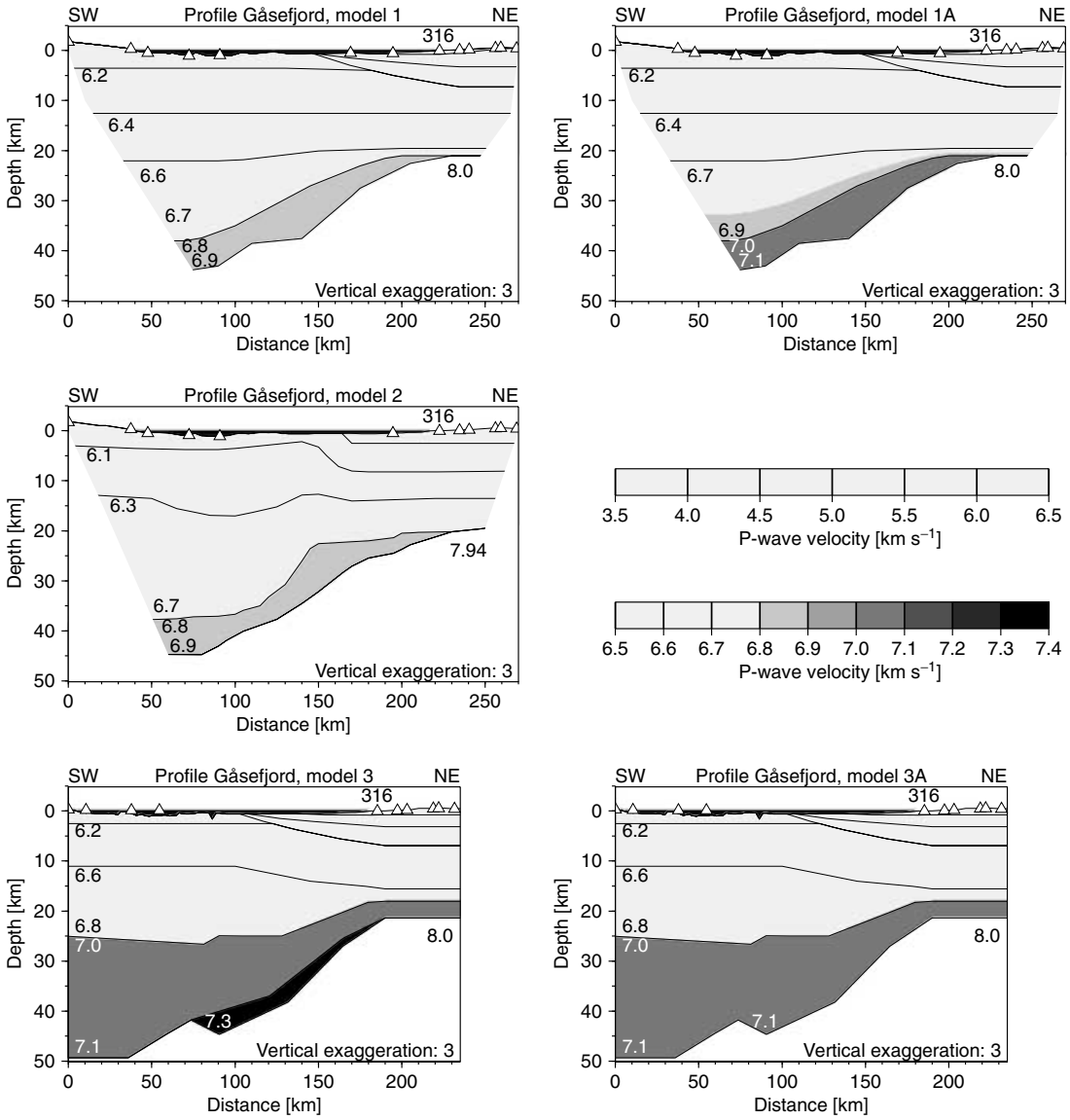

Figure 18. *P*-wave velocity models A–E for the Gåsefjord profile (AWI-90300/310 and 94400): 1, this paper; 1A, this paper with high-velocity lower crust; 2, Schlindwein & Jokat (1999); 3, Mandler & Jokat (1998); 3A, Mandler & Jokat (1998) without underplating. Some velocity values (in km s^{-1}) are noted. Triangles mark the locations of the receiver stations. The vertical exaggeration is ×3. Note the differences in the lower crust.

profited from the reviews of T. Dahl-Jensen and E. Flueh and from the annotations made by G. Eagles and V. Schlindwein. All figures were created with GMT (Wessel & Smith 1998).

REFERENCES

Bohlen, T., 2002. Parallel 3-d viscoelastic finite difference seismic modelling, *Comput. Geosci.,* **28,** 887–899.

Carbonell, R. *et al.,* 1996. Crustal root beneath the Urals: wide-angle seismic evidence, *Science,* **274,** 222–224.

Christensen, N. & Mooney, W., 1995. Seismic velocity structure and composition of the continental crust: a global view, *J. geophys. Res.,* **100**(B7), 9761–9788.

Durrheim, R. & Mooney, W., 1994. Evolution of the Precambrian lithosphere: seismological and geochemical constraints, *J. geophys. Res.,* **99**(B8), 15 359–15 374.

Escher, J. & Pulvertaft, T., 1995. *Geological map of Greenland, 1:2 500 000,* Geological Survey of Greenland, Copenhagen.

Fechner, N. & Jokat, W., 1996. Seismic refraction investigations on the crustal structure of the western Jameson Land Basin, East Greenland, *J. geophys. Res.,* **101**(B7), 15 867–15 881.

Henriksen, N., Higgins, A., Kalsbeek, F. & Pulvertaft, T., 2000. Greenland from Archaean to Quaternary; descriptive text to the geological map of Greenland, 1:2 500 000, *Geol. Greenland Surv. Bull.,* **185,** 1–93.

Jokat, W. *et al.,* 1995. Seismic refraction, in, *Die Expedition ARKTIS-X/2 mit FS 'Polarstern' 1994,* Report on Polar Research 174, ed. Hubberten, H.-W., Alfred Wegener Institute for Polar and Marine Research, Bremerhaven, Germany.

Jokat, W. *et al.,* 1996. Marine Geophysik, in, *Die Expedition ARKTIS-VII/3 mit FS 'Polarstern' 1990,* Report on Polar Research 189, ed. Miller, H. & Grobe, H., Alfred Wegener Institute for Polar and Marine Research, Bremerhaven, Germany.

Larsen, H., 1990. The East Greenland Shelf, in, *The Arctic Ocean Region,* The Geology of North America Vol. L, pp. 185–210, ed. Grantz, A., Johnson, K. & Sweeney, J., The Geological Society of America, Boulder, CO.

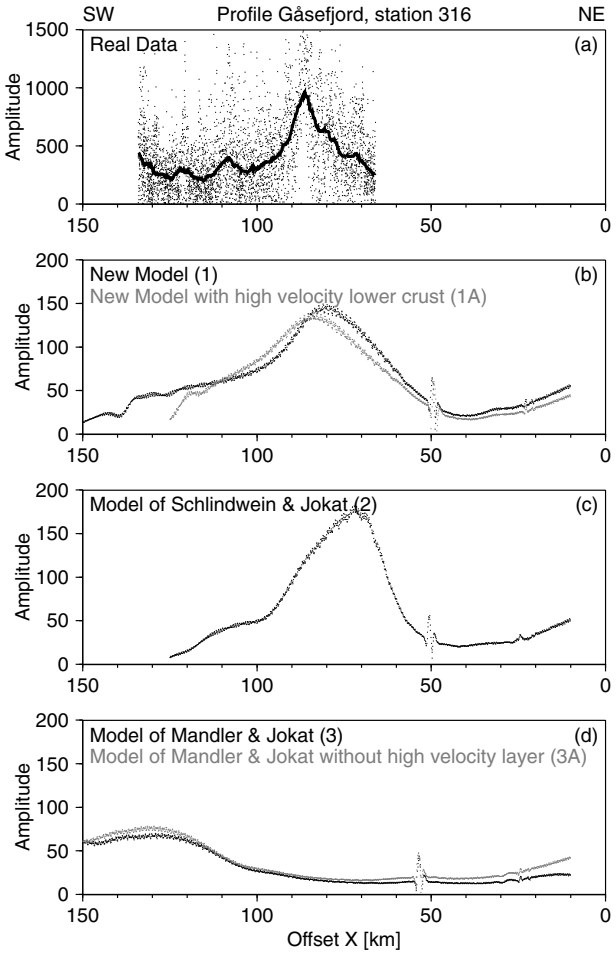

Figure 19. Amplitude characteristics of the *PmP* phase of station 316 (Gåsefjord profile). (a) Real data. Dots represent single amplitudes, the bold line shows the curve calculated with a median filter (5 km). (b)–(d) Synthetic FD data for different models. No filtering was applied.

Larsen, H. & Marcussen, C., 1992. Sill-intrusion, flood basalt emplacement and deep crustal structure of the Scoresby Sund region, East Greenland, in *Magmatism and the Causes of Continental Break-up,* Geological Society of London Special Publication 68, pp. 365–386, ed. Storey, B., Alabaster, T. & Pankhurst, R., The Geological Society, London.

Mandler, H. & Jokat, W., 1998. The crustal structure of Central East Greenland: results from combined land-sea seismic refraction experiments, *Geophys. J. Int.,* **135,** 63–76.

Meissner, R., 1986. *The Continental Crust—A Geophysical Approach,* International Geophysics Series Vol. 34, Academic Press, New York.

Musacchio, G., Mooney, W. & Luetgert, J., 1997. Composition of the crust in the Grenville and Appalachian provinces of North America inferred from V_P/V_S ratios, *J. geophys. Res.,* **102**(B7), 15 225–15 241.

Saunders, A., Fitton, J., Kerr, A., Norry, M. & Kent, R., 1997. The North Atlantic igneous province, in *Large Igneous Provinces,* AGU Geophysical Monograph 100, pp. 45–93, eds Mahoney, J. & Coffin, M., American Geophysical Union, Washington, DC.

Schlindwein, V. & Jokat, W., 1999. Structure and evolution of the continental crust of northern east Greenland from integrated geophysical studies, *J. geophys. Res.,* **104**(B7), 15 227–15 245.

Schlindwein, V. & Jokat, W., 2000. Post-collisional extension of the East Greenland Caledonides: a geophysical perspective, *Geophys. J. Int.,* **140,** 559–567.

Schlindwein, V. & Meyer, U., 1999. Aeromagnetic study of the continental crust of northeast Greenland, *J. geophys. Res.,* **104**(B4), 7527–7537.

Schmidt-Aursch, M. & Jokat, W., 2005. The crustal structure of central East Greenland—II: from the Precambrian shield to the recent mid-oceanic ridges, *Geophys. J. Int.,* doi: 10.1111/j.1365-246X.2005.02515.x (this issue).

Weigel, W. *et al.,* 1995. Investigations of the East Greenland continental margin between 70° and 72°N by deep seismic sounding and gravity studies, *Mar. geophys. Res.,* **17,** 167–199.

Wessel, P. & Smith, W., 1998. New, improved version of Generic Mapping Tools released, *EOS, Trans. Am. geophys. Un.,* **79**(47), 579.

Zelt, C. & Smith, R., 1992. Seismic traveltime inversion for 2-D crustal velocity structure, *Geophys. J. Int.,* **108,** 16–34.